Vol. 27 • No. 18 • May 13 • 2015

www.advmat.de

ADVANCED MATERIALS

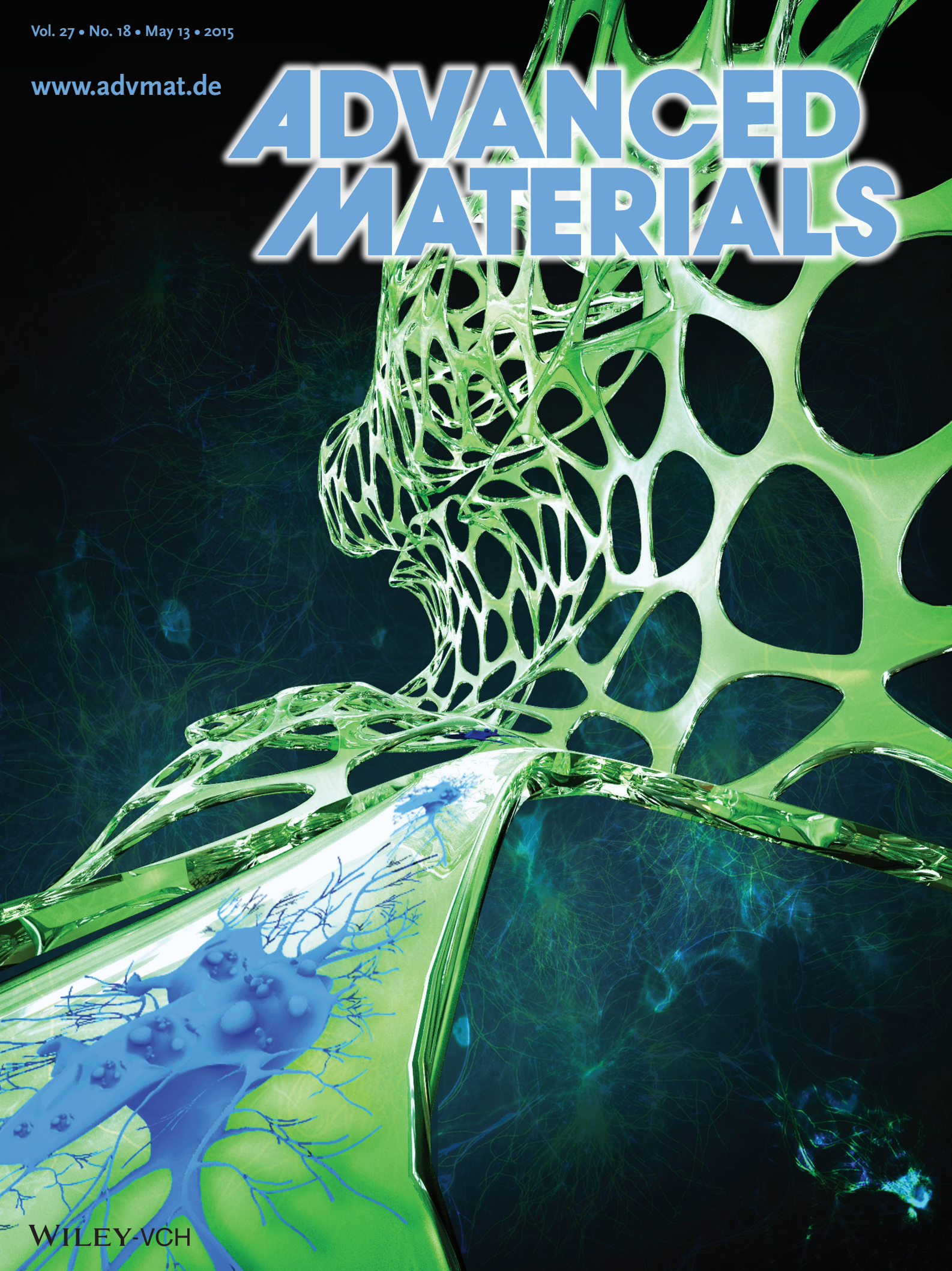

WILEY-VCH

Self-Organizing Large-Scale Extracellular-Matrix Protein Networks

Seungkuk Ahn, Leila F. Deravi, Sung-Jin Park, Borna E. Dabiri, Joon-Seop Kim, Kevin Kit Parker, and Kwanwoo Shin**

Protein fibrillogenesis is a critical self-assembly process that leads to the formation of the extracellular matrix (ECM), propagating tissue-genesis and homeostasis in vivo.[1–4] It involves the organization and polymerization of molecules into fibrils through a combination of the chemical, physical, and mechanical coupling. In the body, proteins undergo fibrillogenesis in the presence of cells, proteoglycans (PGs), and other small molecules to form the heterogeneous, connective ECM networks. Mimicking the fibrillar structure of the ECM in vitro represents an important technological hurdle in tissue engineering, as the exact mechanism behind protein fibrillogenesis remains unknown. What is known is that ECM proteins such as fibronectin (FN), collagen (COL), laminin (LAM), and elastin (ELAS) are fibrillar components of the ECM and that polyanionic PGs rich in sulfonic acid side groups, such as chondroitin sulfate and heparin sulfate, coordinate and couple to the glycoproteins to stabilize network structure required for healthy cell and tissue function.[1,3–6]

Previous attempts have been made to explain the role of mechanical and electrostatic forces on protein fibrillogenesis in vitro.[7–20] Feinberg and co-workers developed highly ordered FN nanofabrics and fibers using a surface-initiated assembly technique, and later work suggested that conformational unfolding of molecular FN occurs to induce its polymerization in vitro.[7,21] Ulmer et al. observed that an external shear-force on hydrophobic micropatterned pillars could induce conformational unfolding in FN, driving the formation of a freely suspended FN network.[8] In a separate study, Pernodet et al. used highly charged polymer surfaces with charge densities equivalent to or higher than the cell's surface charge (0.10 C m^{-2}) to initiate FN unfolding and spontaneous fibrillogenesis.[9] More recently, Ballester-Beltran and co-workers showed that exposing FN molecules to specific surface chemistries also induced FN fibril assembly.[10,11] Collectively, these data suggest that both external mechanical forces and electrostatic charges may trigger the conformational changes in FN required for fibrillogenesis.

While considerable efforts have been devoted to manufacturing FN fibers and fabrics in vitro using mechanical or electrostatic cues separately, little is known about how local distributions of PGs influence protein conformation, organization, and polymerization. Material techniques of surface patterning, however, have afforded a unique way for bio-related studies; physiochemical and biological properties of cells can be regulated by the surrounding ECM components.[22] To investigate the role of protein secondary structure in PG-induced fibrillogenesis, we micropatterned polyelectrolyte islands that mimic the negative charges of the PGs and used these substrates to initiate polymerization of a randomly distributed protein suspension. We hypothesize that soluble glycoproteins can be mechanically unfolded upon contact with artificially distributed PG mimetics and that these conformational changes enable the formation of highly organized fibril network along the charged nodes. To test this hypothesis, we varied the size and the shape of the polyelectrolyte patterns used as a PG mimetic and observed how alterations to surface topography and proximity of charges impacted network formation. We also examined whether other fibrillar ECM proteins beyond FN, such as COL, LAM, and ELAS self-organize and assemble in the presence of charged nodes. Our data reveal a novel bottom-up method to form anisotropic, free-standing protein networks to be used as flexible, transferrable substrates for cardiac and neuronal tissue engineering.

To build PG mimetic islands, we used polystyrene sulfonate acid (PSS), an anionic derivative of polystyrene (PS), as a biomimetic analogue to negatively charged sulfonated PGs such as heparin sulfate.[9,23–26] PSS contains a variable number (16–44 mol%) of sulfonate groups, which are covalently bound to the aromatic rings of polystyrene. To determine if the negative charges on PSS can initiate protein unfolding and polymerization, we initially monitored changes in the protein's secondary structure by using variously charged PSS isotropic films. We incubated the films in FN-containing buffer solution for 72 h and used real-time Fourier-transform infrared (FTIR) spectroscopy to characterize changes in the position of the amide I peak (**Figure 1**a). Note that the corresponding full spectra of Figure 1a,b are shown in the Supporting Information (Figure S1 and S2, respectively). The shift in the amide I peak is an important indicator of FN's secondary structure, suggesting either a compact conformation (wavenumber > 1640 cm^{-1}) or an extended conformation (wavenumber < 1640 cm^{-1}). We observed, however, no noticeable changes

S. Ahn, Prof. K. Shin
Department of Chemistry and Institute of Biological Interfaces
Sogang University
Seoul 121-742, Republic of Korea
E-mail: kwshin@sogang.ac.kr
Dr. L. F. Deravi, Dr. S.-J. Park, B. E. Dabiri, Prof. K. K. Parker
Disease Biophysics Group
Harvard School of Engineering and Applied Sciences
Cambridge, MA 02138, USA
E-mail: kkparker@seas.harvard.edu
Prof. J.-S. Kim
Department of Polymer Science and Engineering and BK21 Education Center of Mould Technology for Advanced Materials and Parts
Chosun University
Gwangju 501-759, Republic of Korea

DOI: 10.1002/adma.201405556

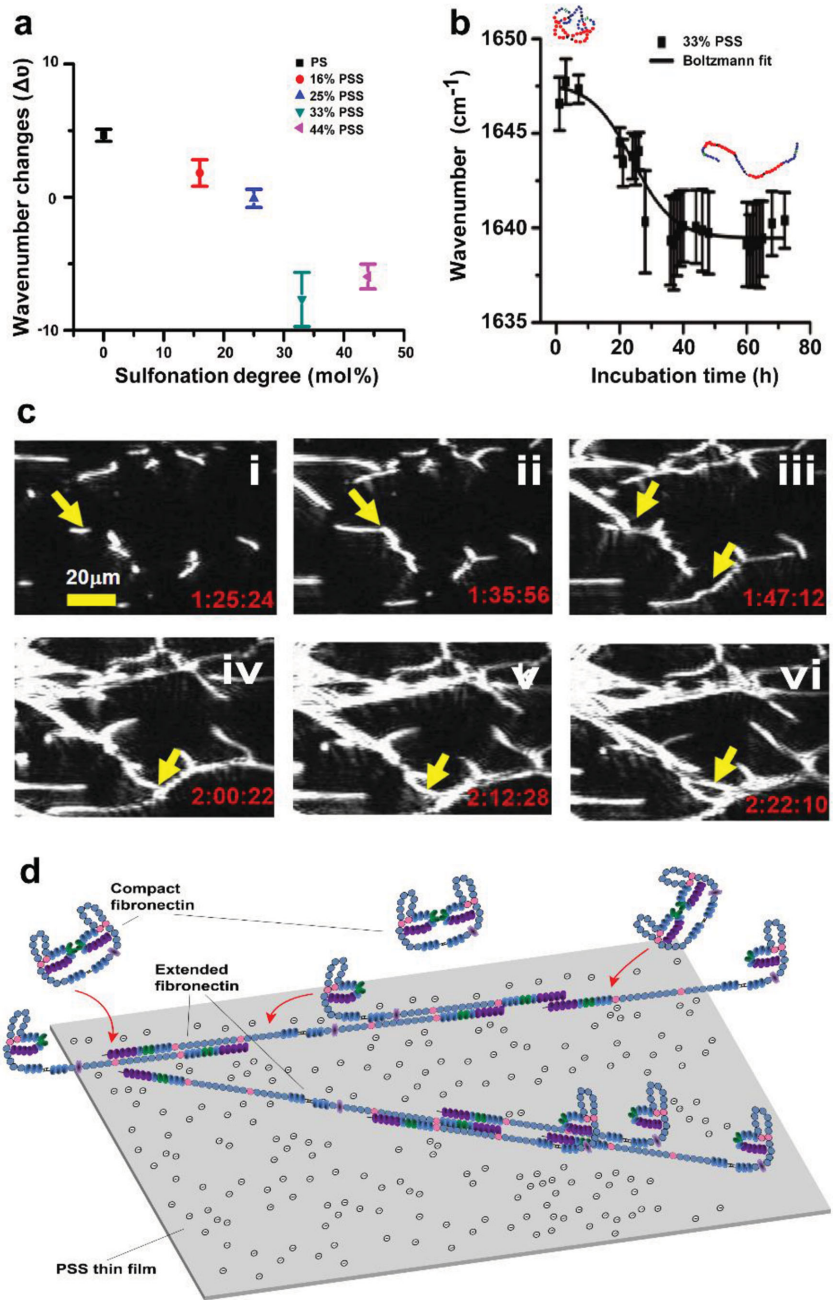

Figure 1. a) Deconvoluted FTIR peaks at 1645 cm^{-1} are shifted toward lower wavenumbers in the case of highly sulfonated PS (>33%). The error bars show the standard deviations ($n = 3$). Mean (SD) wavenumber changes for PS, 16% PSS, 25% PSS, 33% PSS, and 44% PSS were 4.7 (± 0.45), 1.8 (± 0.99), –0.088 (± 0.68), –7.7 (± 2.0), and –6.0 (± 0.93), respectively. b) In situ tracking of the FTIR amide I peaks during FN network formation ($n = 3$). The red shift in the region of 1635–1650 cm^{-1} on the 33% PSS surfaces is indicative of protein unfolding. The secondary structure in the protein transitions from a disordered structure (>1640 cm^{-1}) to a β-sheet structure (<1640 cm^{-1}). The Boltzmann function in the Origin program was used to fit the nonlinear data in order to show a sigmoidal change. c) In situ monitoring of FN fibril formation upon a randomly coated PSS thin film by using imaging ellipsometry. The yellow arrows represent points where new FN fibers and fiber connections emerge, and the measurement times after the incubation are indicated on each figure. The scale bar is 20 μm. d) Schematic representation of FN fibril formation on a highly charged PSS thin film.

in the amide I peak for FN incubated on polymer films containing <25% sulfonation (Figure 1a), suggesting FN does not undergo the conformational changes necessary for polymerization to occur. When films contain >25% sulfonation, however, the position of the amide I peak decreases from 1646 to 1639 cm^{-1} up on the incubation, which is observed in the negative change in the wavenumber in Figure 1b. This result is in agreement with the results observed by Pernodet et al.;[9] they estimated that the minimum charge density required to form a distinct fibril network was 18%, equivalent to ≈0.12 C m^{-2}. Collectively, these data suggest that negative charges above 25% initiate FN conformational unfolding, a step which is critical for fibrillogenesis to occur.

To identify whether protein unfolding initiates fibrillogenesis along the charged films, we used in situ imaging ellipsometry (Figure 1c). This technique enables the real-time detection of fiber formation by measuring changes in the polarization of light reflected from the surface and imaged by a CCD camera.[27,28] Here, a glass coverslip is coated with an isotropic layer of highly charged PSS, and FN is incubated on its surface. We observed the initiation of fiber formation (Figure 1c(i)) and the progressive elongation and thickening of fibers over a period of 2 h (Figure 1c(ii)–(vi)). The newly formed fibers, which have higher refractive indices due to the bundling of fibrils, grow in the direction of the long axis of the fiber, suggesting three steps for fibril formation as schematically described in Figure 1d: i) initiation upon the adsorption of the compact FN molecules on the highly charged surface, ii) unidirectional extension of the unfolded FN molecules, and iii) transverse bundling of the extended FN molecules, resulting in the thickening of the fibers.

We asked whether anisotropic networks of FN could be formed along micropatterned nodes enriched in PSS with greater than 25% sulfonation. To test this, we incubated soluble FN along a micropatterned array as detailed in **Figure 2**a and illustrated in Figure 2b. We used fluorescently labeled FN to follow network formation for over 14 h. Networks formation is initiated at the micropatterned 33% PSS nodes, which we predict to have the highest initial concentrations of selectively adsorbed FN, as indicated by the high fluorescence at the nodes (Figure 2a(i)). After FN adsorption, the coated patterns were incubated in a 0.5% (v/v) polyvinyl alcohol (PVA) solution for 48 h at 37 °C, and network was observed to form spontaneously over time (Movie S1, Supporting Information). PVA reduces the surface tension of widespread FN thin layers, thereby increasing the

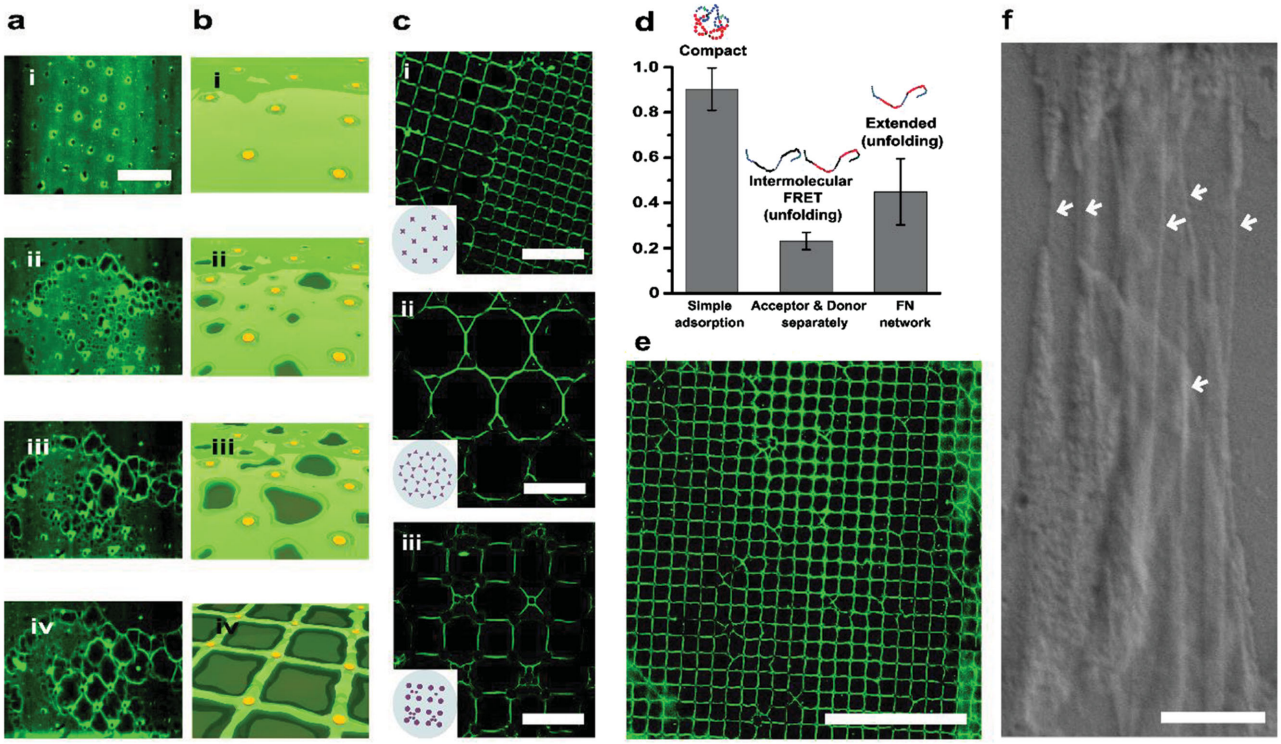

Figure 2. Fibrillar FN networks formed on PSS nodes. a) Real-time confocal images show that FN network formation is initiated along the 33% PSS nodes during incubation with PVA for (i) 0 h, (ii) 8 h, (iii) 9 h, and (iv) 14 h. The scale bar is 100 μm. b) Schematic of network formation. Micropatterned PSS islands on glass are shown in yellow while FN is shown in green. c) Variations in the patterned PSS islands during network formation. The schematics in the lower left corners (in purple) show the shapes of the PSS micropatterns. The FN networks can be seen to form on a variety of patterns, including (i) square patterns with 20 μm (right) and 40 μm pitches (left), (ii) hexagonal patterns, and (iii) sporadic patterns. The scale bars are 400 μm (i) and 100 μm (ii and iii). d) Statistics of the intensity ratio of acceptor to donor indicate that FN is extended in networks. The error bars show standard deviation ($n = 3$, 100 points, mean and SD of simple adsorption on PS were 0.90 and 0.094. Mean and SD of intermolecular FRET from FN labeled with acceptor and donor separately were 0.23 and 0.038, whereas those of FN network samples were 0.45 and 0.15, respectively. e) Large scale of FN networks. The scale bar is 500 μm. f) SEM image of FN networks. The scale bar is 2 μm.

mobility of FN molecules adsorbed on the substrate.[8] These properties result in the formation of highly ordered networks suspended across the patterns (Figure 2a(ii)–(iv), illustrated in Figure 2(ii)–(iv)). These data suggest that in the presence of PVA, FN molecules undergo a parallel dewetting-like motion and that connections spontaneously form between the PSS patterns.

Surface-charge-initiated protein unfolding along isotropically coated polymer surfaces has been previously established.[9–15] However, we report the first use of micropatterned PSS to induce spontaneous formation of homogeneous long-range protein networks. When PVA is used, the physically adsorbed proteins are localized between the negatively charged islands and polymerized to form suspended fibers. This phenomenon is somewhat similar to the instability, dewetting, and/or hole formation of a polymer thin film on a patterned solid substrate when the layer confined between two media (water and the substrate) is spinodally unstable.[29–31] As shown in Figure 2a and Movie S1, Supporting Information, the densely adsorbed FN evolved to abruptly form precisely organized FN fibers between the PSS patterns. After incubation for 14 h (Figure 2a(iv)), adjacent rims from the ruptured areas in the sample coalesced into square-shaped networks between the PSS spots. The dewetting-like ruptured holes stop at the lines of the shortest distance between the spots, and the fibers extend from the areas of aggregated protein closest to the micropatterned nodes. As a result, large-scale, self-organizing FN networks are formed over a mm^2-scale area. The schematics of the network formation are visualized in Figure 2b.

Fluorescence confocal microscopy revealed that the formed networks are dependent on both the available surface charge (Figure S3, Supporting Information) and the distribution of available surface charges (Figure S4, Supporting Information). For instance, FN networks do not form along positively charged micropatterns or micropatterns with sulfonated charges <25% (Figure S3a,b, Supporting Information). Our data suggest that networks self-organize only when incubated along PSS patterns with sulfonation >33% (Figure 2c and Figure S3c, Supporting Information), indicating that charge-induced initiation must occur prior to network formation. Another important parameter in potentiating network formation is the distance between PSS points. FN networks were formed only when micropatterns were between 20 and 40 μm apart (Figure S4a,b, Supporting Information). At distances >40 μm, FN fibers did not form continuous networks (Figure S4c,d, Supporting Information). Note that higher PSS concentration did not allow to form FN networks in longer distances between islands (Figure S4e–l, Supporting Information). These data suggest that both charge

density and spatial proximity of charged islands are necessary to regulate the network connection.

If the composition and the distribution of negative charges control network formation, then the periodicity and the morphology of the protein network should also be controlled to build an array of patterns. To test this hypothesis, we varied the micropatterned PSS islands to form complex structures containing varying grid intervals of 20 and 40 μm (Figure 2c(i)), hexagons (Figure 2c(ii)), and combinations of the two (Figure 2c(iii)). Regardless of the pattern, FN fibrils were formed only at regions between the shortest distances, suggesting that the growth of FN fibers is guided by adjacent PSS nodes.

We asked whether the anisotropic networks are composed of fibrillar FN. If fibrillogenesis is to occur, FN must undergo conformational unfolding from a soluble compact conformation to an insoluble extended conformation.[32–35] To identify conformational changes in FN during network formation, we also used fluorescence resonance energy transfer (FRET) (Figure 2d). As previously observed by in situ FTIR in Figure 1b and Figure S2, Supporting Information, the negative shift in the wavenumber suggests a conversion of the secondary structure from a compact to an extended conformation during network formation.[36] This finding was also supported by the FRET analysis (Figure 2d and Figure S5, Supporting Information), wherein FN molecules were dual-labeled with acceptor and donor fluorophores according to previously published protocols.[7,37–39] In these experiments, the FRET signal is defined by the ratio between the intensity of the acceptor (I_A) and the intensity of the donor (I_D). Low FRET signals ($I_A/I_D < 0.5$) represent an extended FN conformation whereas high FRET signals ($I_A/I_D > 0.5$) suggest a compact FN. Here, we show that FN is in an extended conformation when it is in the formed networks and that it is in a compact conformation ($I_A/I_D = 0.90$) when it is in solution (Figure 2d and Figure S5, Supporting Information). Intermolecular fluorescence ($I_A/I_D = 0.23$) was measured to ensure that the observed FRET signals are primarily associated with intramolecular conformational changes. Both in situ FTIR and FRET analysis suggest that FN is polymerized within the networks due to conformational changes and that this polymerization is responsible for the stability of the networks. Note that the desired FN networks can be achieved to large areas up to ≈mm^2 (Figure 2e) using this method, which is of great importance in practical device applications, such as scaffolds for tissue engineering.

We asked whether the formed networks are freely suspended across the micropatterned nodes. To test this, we incubated FN-coated paramagnetic beads with the formed networks (Figure S6a, Supporting Information). Custom-built magnetic tweezers were used to generate a localized magnetic field in order to generate ≈450 pN per bead during 4 s.[40] In this setup, the bead-bound fiber was pulled toward the origin of the magnetic field (Figure S6b, Supporting Information). When the magnetic field was removed, the strained fiber returned to its original position (Figure S6c,d and Movie S2, Supporting Information), suggesting that the fibers were freely suspended across the PSS nodes. To further investigate the topology of the freely suspended fibers within the network, we used scanning electron microscopy (SEM). The FN fibers had an average diameter of 5.54 μm ($n = 3$, points = 100, standard deviation = 1.51 in Figure 2f). Collectively, these data reveal that the fibers are composed of a flat, ribbon-like composition that are transversely suspended between the PSS nodes.

Given the self-organizing properties of FN along the PSS nodes, we next asked whether other fibrillar β-sheet-rich ECM proteins can assemble to form free-standing networks across micropatterned PSS. Note that FN, LAM, and ELAS all contain secondary structures rich in β-strands (47%, 15%, and 36%, respectively, in total amount of secondary structures),[41–44] but COL contains a secondary structure rich in α-helices (40% in total amount of secondary structures).[45,46] In vivo, FN and LAM form networks through receptor-triggered self-assembly, whereas ELAS and COL require chemical crosslinking for fibrillogenesis.[32,47–49] FN and COL are also present throughout the body, but LAM and ELAS are localized primarily to the basement membrane and connective tissue, respectively.[33,47,50,51] We, therefore, tested the ability of LAM, another β-sheet-rich ECM protein, and those of type-1 COL and ELAS, both of which are β-sheet-poor ECM proteins, as controls. As shown in **Figure 3**a and Figure S7e, Supporting Information, LAM assembled into self-organizing networks on highly charged PSS, similar to FN; however, COL and ELAS (Figure S7a,c, Supporting Information) did not form continuous networks on PSS islands. COL networks do form only when incubated with FN, but ELAS networks do not. This is because FN has a binding subunit for COL, but not for ELAS.[32] Also, FN is usually coupled with type-1 COL in tissues.[32]

FN and LAM are well known to bind selectively to an integrin receptor or heparin sulfate in vitro, resulting in the formation of insoluble fibers via cell-mediated fibrillogenesis.[1,32–35,41] On the other hand, COL and ELAS are often coupled with other proteins in their fibrillar form. When COL is coated on pre-existing FN networks, composite fibers are formed (Figure 3b). This coupling between FN-COL is also seen when FN is incubated with pre-existing isotropic COL coated the PSS patterns. FN did not follow morphological cues from the PSS patterns; instead, FN followed cues from the pre-existing isotropic COL, showing the strong nature of the FN-COL interaction (Figure S7b, Supporting Information).[1,32] We also observe that LAM multifi-

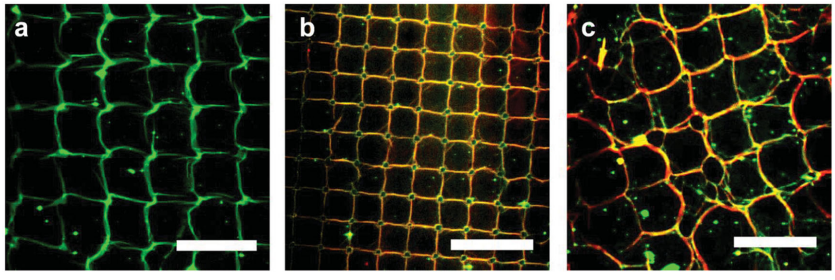

Figure 3. Diverse ECM fibers on PSS micropatterns for various ECM proteins: a) 33% PSS induced laminin network. The scale bar is 200 μm. b) Collagen (red) surface coating on pre-existed FN network (green) by post collagen incubation. The scale bar is 100 μm. c) Laminin multifibril (green) on pre-existed FN network (red) by post laminin incubation. The scale bar is 100 μm.

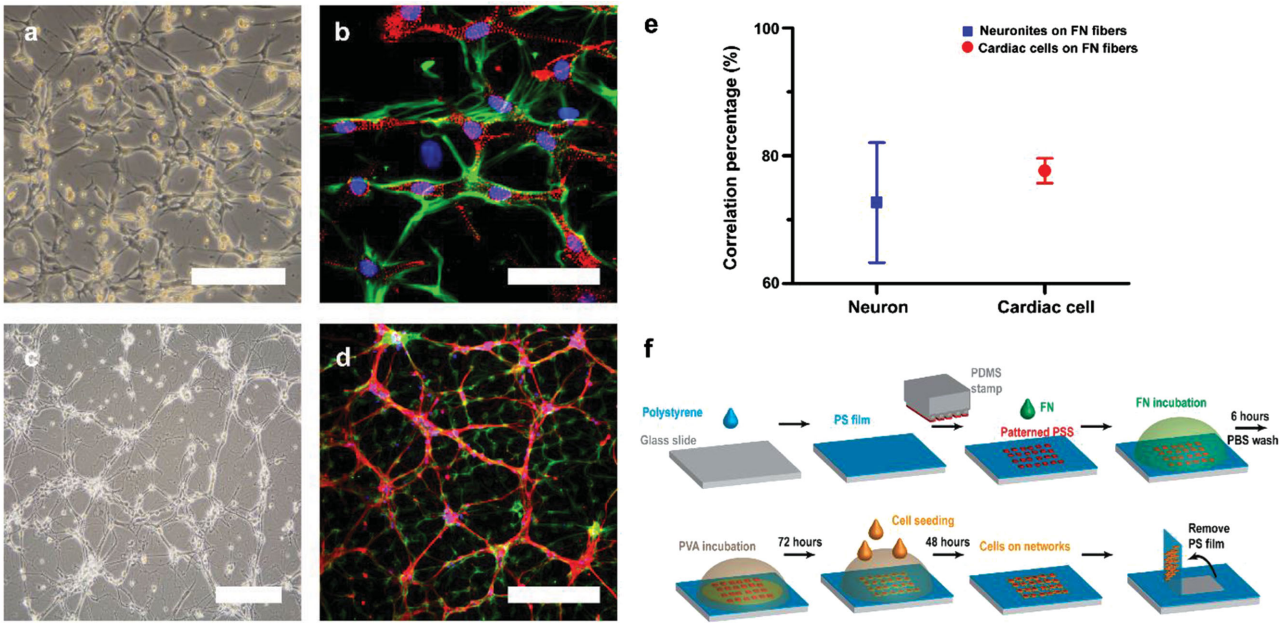

Figure 4. Bright field image (a) and confocal image (b) of FN networks (green) on 33% PSS islands cultured with cardiomyocytes during 3 d, stained for the nucleus (DAPI, blue), α-actinin (monoclonal α-actinin, red). The scale bars for (a) and (b) are 100 and 50 μm, respectively. Bright field image (c) and confocal image (d) of FN networks (green) on 33% PSS islands cultured with neuron cells during 7 d, stained for the nucleus (DAPI, blue), neuronal networks (β3-tubulin, red). The scale bars are 200 μm. e) Quantitative analysis of the percentage of α-actinin (red) and β3-tubulin (blue) co-localized with FN fiber. Error bars show standards (n = 5). Mean (SD) correlation percentages for β3-tubulin in neurons (blue) and α-actinin in cardiac cells (red) were 73 (± 9.4)% and 78 (± 1.9)%, respectively. f) Schematic depiction of the removal of a free-standing film with cells adsorbed in FN networks from its substrate.

brils form on the top of pre-existing FN networks (Figure 3c) to form composite networks. Unlike COL or LAM, ELAS fibers do not form on the pre-existing FN networks (Figure S7d, Supporting Information). We believe this is due to ELAS behavior in vivo. It has no interaction with FN. These data suggest that both secondary structure and the native function of the proteins regulate its ability to undergo polymerization into networks.

To assess the biocompatibility of the networks, we asked whether they can recruit and align cells. We cultured the FN networks with neonatal rat ventricular myocytes and rat primary cortical neuronal cells. Cardiomyocytes grew selectively along and through fibers in the networks (**Figure 4**a,b) but were randomly distributed on an isotropic FN surface (Figure S8a,b, Supporting Information). The cardiomyocytes cultured with FN networks spontaneously contracted (Movie S3, Supporting Information), suggesting the cells are coupled together along the free-standing networks. The cardiomyocytes formed and maintained sarcomeres on the FN network. This suggests that the FN network is pre-stressed and capable of supporting the cyclic stresses associated with cardiac contractility.[52] The neonatal cortical neuronal cells adhered to the network and extended neurites along the FN fibers (Figure 4c,d). As shown in Figure 4e, 78% and 73% of 2D cross-correlation percentages of α-actinin in cardiac cells and β3-tubulin in neurons with FN fibers to intensities of FN fibers, respectively, are indicating that the FN networks are guiding those cellular growths along the FN fibrils and robust enough to support fundamental mechanisms of tissue genesis.

The versatility of the free-standing FN networks was further demonstrated, as they were formed on detachable PS films (Figure 4e and Movie S4, Supporting Information). Once detached, the PS-network films could be transferred to other 3D substrates, such as an aluminum mandrel (Movie S5, Supporting Information). In addition, both cardiomyocytes and neonatal cortical neurons were cultured on the PS/network films and released into buffer solutions (Figure 4c and Figure S8c, Supporting Information). We show that this release process does not damage the network structure or cellular function (Movie S4 and S6, Supporting Information). For instance, cardiomyocytes on the transferrable FN networks spontaneously contracted before and after release. This application suggests that we can build ECM network-cell sheet without significant loss of any biological function.

In this report, we described how PG mimetics not only recruit but also stabilize fibrillar ECM proteins and show that this process depends on the protein's secondary structure. We found that the spontaneous, highly ordered large-scale (up to mm^2) ECM network formation. Once formed, the chemical and the biological functionalities of the networks were investigated. Our data suggest that a mechanism consisting of four steps can be hypothesized based on our observations and the aforementioned references. First, FN binding to highly charged domains induces protein unfolding due to a strong electrostatic interaction with the sulfonic groups exposed from the PSS. Second, an increase in the concentration of FN near the unfolded FN at the PSS spots leads to molecular assembly, which forms a cluster of fibrillated FN molecules and becomes a node for the FN network. Third, once a fibril is formed, other FN molecules in the FN solution are sequentially connected to it. Finally, during the post-incubation step, the adsorbed FN film is ruptured at the substrate and connected to the fibrillated FN domains.

Together, these data suggest that by mimicking the PG surface charges, we can build anisotropic, fibrillar FN networks. We further demonstrated applications of these networks to template the formation of ECM composite fibers and cell patches. Collectively, our results suggest that proteins that are endowed with β-sheet molecular domains and do not require external crosslinking to form insoluble fibers are capable of self-assembling into networks and that these precisely controlled connections provide a flexible, transferable substrate customized for tissue engineered cardiac and neuronal scaffolds.

Experimental Section

Chemicals: Systematic studies of the FN fibril formation on polyelectrolyte patterns were carried out using several weakly charged random copolymers. Polystyrene represented the neutral charge and was purchased from Polymer Source. Poly(styrene-*ran*-styrene sulfonic acid) with various degrees of sulfonation ranging from 4 to 44 mol% were prepared by using the sulfonation method developed by Makowski and co-workers and were purchased from Polymer Source.[53] The synthesized copolymers were characterized using gel permeation chromatography (GPC) and ^{1}H-NMR. The complete specifications of the polymers used are listed in **Table 1**.

FN Fibrillogenesis on Randomly Charged Surfaces: PS (Sigma–Aldrich), poly(styrene-*co*-4-styrene sulfonic acid) (PSS15, mol% of SO3H: 15.9, Polymer Source), poly(styrene-*co*-4-styrene sulfonic acid) (PSS25, mol% of SO3H: 25.1), poly(styrene-*co*-4-styrene sulfonic acid) (PSS33, mole% of SO3H: 33.0, Polymer Source), and poly(styrene-*co*-4-styrene sulfonic acid) (PSS44, mol% of SO3H: 44.0, Polymer Source) were dissolved in dimethylformamide (DMF). Then, glass coverslips were spin-coated with the polymer solutions at 2000 rpm for 1 min. The spin-coated surfaces were annealed at 100 °C overnight and incubated with 66 μg mL^{-1} FN in PBS for 72 h at 37 °C. After incubation, samples were washed three times in phosphate-buffered saline (PBS) (pH 7.4).

Photolithography and Microcontact Printing: L-Edit (Tanner EDA) was used to design photolithographic masks. Silicon wafers (Wafer World) were spin-coated with an SU-8 2002 photoresist (MicroChem Corp.) and were put under photomasks while being exposed to UV light from a mask aligner (ABM, Inc.). In order to dissolve the masked regions, we immersed the wafers in propylene glycol methyl ether acetate.[54,55] Polydimethylsiloxane (PDMS) (Sylgard 184, Dow Corning) stamps were fabricated by using wafers as templates and were coated for 2 h at room temperature with 20 μg mL^{-1} PSS33 dissolved in 50% DMF and 50% PBS solutions for FN network formation and with PSS16 dissolved in 50% DMF and 50% PBS solutions for control samples. Then, the inking solutions were removed by air blowing and the stamps were placed in contact with the glass coverslips that had been treated in a UV–ozone cleaner (Jelight Company, Inc.). After 1 h stamping, the patterned coverslips were stabilized in an oven at 37 °C.

Table 1. Characteristics of the random polyelectrolytes used in this study.

Designation	Sample	M_w [g mol^{-1}]	M_w/M_n
PS	Polystyrene	280 000	1.05
PSS5	Polystyrene-*ran*-styrene with 5 mol% sulfonic acid	100 000	1.05
PSS10	Polystyrene-*ran*-styrene with 10 mol% sulfonic acid	100 000	1.05
PSS15	Polystyrene-*ran*-styrene with 15 mol% sulfonic acid	300 000	1.05
PSS25	Polystyrene-*ran*-styrene with 25 mol% sulfonic acid	200 000	1.05
PSS33	Polystyrene-*ran*-styrene with 33 mol% sulfonic acid	100 000	1.05
PSS44	Polystyrene-*ran*-styrene with 44 mol% sulfonic acid	100 000	1.08

Formation of FN Networks on Patterned Polymer Surfaces: The patterned coverslips were incubated with 66 μg mL^{-1} FN conjugated with Alexa Fluor 488 carboxylic acid, 2,3,5,6-tetrafluorophenyl ester (Molecular Probes, Invitrogen), or tetramethylrhodamine-5-maleimide (Molecular Probes, Invitrogen) in PBS for 6 h in an oven at 37 °C. After FN incubation, the coverslips were washed and directly incubated with 0.5% (v/v) PVA (Mowiol 488, Sigma Aldrich) for 48 h at 37 °C.

Real-Time Confocal Imaging: After incubation with 0.5% PVA, real-time confocal (Zeiss LSM 5 LIVE) images were captured every 1 h for 24 h at a controlled temperature (37 °C).

Fluorescence Resonance Energy Transfer: An acceptor fluorophore (tetramethylrhodamine-5-maleimide, Molecular Probes, Invitrogen) and a donor fluorophore (Alexa Fluor 488 carboxylic acid, 2,3,5,6-tetrafluorophenyl ester, Molecular Probes, Invitrogen) were used for the FRET tests.[7,37–39] The labeled protein was purified using size exclusion chromatography (quick-spin protein sephadex columns, Roche Applied Sciences), and the eluent was collected and used for network formation. For the non-specific fluorescence test, FN was separately labeled with the acceptor and donor fluorophore and then mixed together before the FN incubation step.

Magnetic Tweezer Setup and Bead Preparation: M450 Tosyl-activated beads (Invitrogen) were functionalized with 50 μg mL^{-1} of FN overnight. After that time, nonspecific FN binding was avoided by washing the beads by PBS. FN network samples were incubated with 0.5 million beads for up to 1 h. After bead incubation, samples were placed on the microscope stage, and confocal images were captured as magnetic tweezers produced a magnetic field that varied with the applied current.[40] In this experiment, the tweezers were positioned 200 μm away from the beaded fibers and were activated for 4 s. The forces generated by the tweezers were calibrated as was done previously.[40] Briefly, paramagnetic beads were placed in a solution of known viscosity (99% glycerol) and their velocity was used to tabulate forces per Stoke's formula.

Formation of Diverse ECM Protein Networks on Patterned Polymer Surfaces: PSS33-patterned coverslips were incubated with 66 μg mL^{-1} laminin–entactin-free (LAM) (BD Biosciences) in PBS or with 66 μg mL^{-1} ELA from bovine neck ligament (Sigma Aldrich) in PBS or with 50% (v/v) COL type-1 solution from rat tail (Sigma Aldrich) in PBS for 6 h at 37 °C. After incubation, samples were washed and then incubated with 0.5% PVA for 48 h at 37 °C. For stacked ECM networks, FN networks were prepared and incubated with three different ECM proteins, 66 μg mL^{-1} laminin, 66 μg mL^{-1} elastin, or 50% (v/v) collagen, in PBS for 6 h at 37 °C. After incubation, the samples were washed and then incubated with 0.5% PVA for 48 h at 37 °C.

Transferrable FN Network: Glass slides were spin-coated with 20 mg mL^{-1} PS in toluene at 100 rpm for 10 s and then at 1000 rpm for 20 s. Samples were microcontact-printed with PSS33-inked stamps and were stabilized at 37 °C overnight. Patterned samples were incubated with 66 μg mL^{-1} FN in PBS for 6 h at 37 °C. After FN incubation, samples were washed and then incubated with 0.5% PVA for 48 h at 37 °C. After wetting, samples were washed, and the edges of each side were cut by using a blade cutter. The samples were immersed in a petri dish filled with deionized (DI) water to make free-standing PS thin films with FN networks.[56] The floating FN networks on PS thin films were transferred to a mandrel.

Cell Culture and Immunostaining: All protocols for dealing with animals were approved by the Animal Use and Care Committee at Harvard University. Cardiomyocytes and rat primary neuron cells were isolated from two-day-old Sprague–Dawely rats by following previous protocols.[40,57] After cell isolation, FN networks were cultured with cardiomyocyte (100 000 cells cm^{-2}) for 3 d or with rat

primary neuron cells (10 000 cells cm^{-2}) for 7 d. For immunostaining of cardiomyocytes, samples were washed with PBS and incubated with 4% paraformaldehyde (4% PFA) (Electron Microscopy Sciences) and triton-X 100 for 10 min to fix the cells. After cell fixation, samples were washed with PBS and incubated with monoclonal antisarcomeric α-actinin (Sigma) for 2 h. After primary antibody staining, samples were washed with PBS and then incubated with 4′,6-diamidino-2-phenylindole, dihydrochloride (DAPI) (Molecular Probes) and goat-antimouse IgG (H+L) tetramethylrhodamine (GAM 546, Invitrogen) for nuclear and α-actinin staining, respectively. After secondary antibody staining, samples were washed with PBS and mounted on glass slides. For immunostaining of rat primary neuron cells, we washed the samples with PBS and then incubated them with 4% PFA for 15 min. After 4% PFA incubation, samples were washed with PBS and then incubated with 0.5% triton-X for 10 min. After cell fixation, samples were washed with PBS and then incubated with 5% BSA for 30 min to block nonspecific binding. Then, the samples were incubated with a 1:200 dilution of β3-tubulin and DAPI in a 0.5% BSA solution overnight. After primary antibody incubation, samples were washed with 0.5% BSA and incubated with a 1:200 dilution of goat-antirabbit IgG (H+L) tetramethylrhodamine and DAPI in a 0.5% BSA solution for 45 min for neuronal network and nuclear staining, respectively. After secondary antibody incubation, samples were washed with 0.5% BSA and PBS. Finally, the samples were mounted on glass slides.

Confocal Imaging and Image Processing: After the final incubation steps, the coverslips were mounted on a microscope stage and imaged with a Zeiss LSM 5 LIVE confocal microscope by using a 10× objective at 37 °C. Captured images were processed in Image J (NIH).

Scanning Electron Microscopy: SEM (Zeiss Supra 55 VP) was used to acquire high-resolution images of FN networks coated with platinum.

FTIR Spectroscopy: FTIR spectra were collected by using a Cary 660 Spectrometer (Agilent Technologies) with a liquid-jacketed flow cell (Pike Technologies). The resolution of the spectra was 4 cm^{-1} in the 650–4000 cm^{-1} wavenumber region. A total of 128 scans were averaged for each spectrum. A surface was prepared by dropping 0.15 mL of PS, PSS16, PSS33, and PSS44 solutions onto an attenuated total reflection (ATR) crystal made of zinc selenide (ZnSe). The crystal was annealed at 100 °C for 24 h. After annealing, the crystal was placed into the liquid-jacketed flow cell, and a water bath was connected to the flow cell as a temperature control at 37 °C. Then, 50 μg mL^{-1} FN in PBS was injected into the flow cell, and we started to collect the spectrum. The background was subtracted, and a baseline correction was made for each spectrum.

FTIR Imaging Spectroscopy: FTIR spectra were collected by using a Cary 660 Spectrometer and a Cary 620 FTIR Microscope (Agilent Technologies). The resolution of the spectra was 4 cm^{-1} in the 650–4000 cm^{-1} wavenumber region. A total of 128 scans were averaged for each spectrum with Agilent's 64 × 64 Focal Plane Array. The total areas of the FTIR images were 350 μm × 350 μm. For surface preparation, gold-coated silicon wafers were put in a piranha solution, a 7:3 mixture of sulfuric acid and hydrogen peroxide, for 1 h in order to make the wafers hydrophilic. After piranha treatment, the wafers were spin-coated with PS and PSS33 solutions at 2000 rpm for 1 min. Then, the surfaces were annealed at 150 °C for 24 h. The annealed surfaces were incubated with 50 μg mL^{-1} FN for 72 h. After the incubation had ended, the samples were washed and then dried with N_2 gas. Samples were mounted on the stage of a FTIR microscope and FTIR images were collected. Background corrections were made for each measurement, and FTIR images were obtained at 1633 cm^{-1}.

IR Spectral Analysis: Deconvolution and curve fitting were used to decompose the amide band into its constituents for the peak assignment in order to analyze the secondary structures.[36,58,59] Deconvolution was performed by using Resolution Pro FTIR software (Agilent Technologies) with a fixed half-width (W = 15 cm^{-1}) and a fixed enhancement factor (K = 2.4).[42] For curve fitting, a Lorentzian function was applied to each deconvoluted spectrum by using Origin data analysis software (Origin Lab Corporation).

Calculation of Cross-Correlation Percentages of α-Actinin in Cardiac Cells and β3-Tubulin in Neurons with FN Fibers: 2D cross-correlation percentages of α-actinin in cardiac cells and β3-tubulin in neurons with FN fibers were calculated by comparing intensities of α-actinin and β3-tubulin with intensity of FN fibers. An xcorr2 function in MATLAB was used to calculate the 2D cross-correlation.

Supporting Information

Supporting Information is available from the Wiley Online Library or from the author.

Acknowledgements

This work was supported by Sogang University Research Grant, the Nuclear Research R&D Program (2013M2A2A6043677), the Mid-career Researcher Program (2011-0017539), the Advanced Research Center for Nuclear Excellence and Basic Science Research Program (2013R1A1A2010265), Sogang-Harvard Center of the Leading Foreign Research Institute Recruitment Program (2013K1A4A3055268), and CELA-NCRC (2008-0062606) funded by the Ministry of Science, ICT & Future Planning, Korea.

Received: December 4, 2014
Revised: March 9, 2015
Published online: March 31, 2015

[1] C. Frantz, K. M. Stewart, V. M. Weaver, *J. Cell Sci.* **2010**, *123*, 4195.
[2] L. Schaefer, R. M. Schaefer, *Cell Tissue Res.* **2010**, *339*, 237.
[3] T. Rozario, D. W. DeSimone, *Dev. Biol.* **2010**, *341*, 126.
[4] L. F. Deravi, H. M. Golecki, K. K. Parker, *J. Chem. Biol. Interfaces* **2013**, *1*, 25.
[5] S. Sarrazin, W. C. Lamanna, J. D. Esko, *Cold Spring Harbor Perspect. Biol.* **2011**, *3*, a004952.
[6] K. Sugahara, T. Mikami, T. Uyama, S. Mizuguchi, K. Nomura, H. Kitagawa, *Curr. Opin. Struct. Biol.* **2003**, *13*, 612.
[7] L. F. Deravi, T. Su, J. A. Paten, J. W. Ruberti, K. Bertoldi, K. K. Parker, *Nano Lett.* **2012**, *12*, 5587.
[8] J. Ulmer, B. Geiger, J. P. Spatz, *Soft Matter* **2008**, *4*, 1998.
[9] N. Pernodet, M. Rafailovich, J. Sokolov, D. Xu, N. Yang, K. McLeod, *J. Biomed. Mater. Res., Part A* **2003**, *64*, 684.
[10] J. Ballester-Beltrán, M. Cantini, M. Lebourg, P. Rico, D. Moratal, A. J. García, M. Salmerón-Sánchez, *J. Mater. Sci.: Mater. Med.* **2011**, *23*, 195.
[11] J. Ballester-Beltrán, P. Rico, D. Moratal, W. Song, J. F. Mano, M. Salmerón-Sánchez, *Soft Matter* **2011**, *7*, 10803.
[12] D. Gugutkov, G. Altankov, J. C. Rodríguez Hernández, M. Monleón Pradas, M. Salmerón Sánchez, *J. Biomed. Mater. Res., Part A* **2010**, *92A*, 322.
[13] M. Salmerón-Sánchez, P. Rico, D. Moratal, T. T. Lee, J. E. Schwarzbauer, A. J. García, *Biomaterials* **2011**, *32*, 2099.
[14] D. Gugutkov, C. González-García, J. C. Rodríguez Hernández, G. Altankov, M. Salmerón-Sánchez, *Langmuir* **2009**, *25*, 10893.
[15] V. Nelea, M. T. Kaartinen, *J. Struct. Biol.* **2010**, *170*, 50.
[16] E. Freire, T. Coelho-Smpaio, *J. Biol. Chem.* **2000**, *275*, 817.
[17] J. A. Matthews, G. E. Wnek, D. G. Simpson, G. L. Bowlin, *Biomacromolecules* **2002**, *3*, 232.
[18] Y. Li, A. Asadi, M. R. Monroe, E. P. Douglas, *Mater. Sci. Eng. C* **2009**, *29*, 1643.
[19] R. A. Neal, S. G. McClugage III, M. C. Link, L. S. Sefcik, R. C. Ogle, E. A. Botchwey, *Tissue Eng., Part C* **2008**, *15*, 11.

[20] L. Buttafoco, N. Kolkman, P. Engbers-Buijtenhuijs, A. Poot, P. Dijkstra, I. Vermes, J. Feijen, *Biomaterials* **2006**, *27*, 724.
[21] A. W. Feinberg, K. K. Parker, *Nano Lett.* **2010**, *10*, 2184.
[22] X. Yao, R. Peng, J. Ding, *Adv. Mater.* **2013**, *25*, 5257.
[23] D. L. Rabenstein, *Nat. Prod. Rep.* **2002**, *19*, 312.
[24] J. T. Gallagher, M. Lyon, W. P. Steward, *Biochem. J.* **1986**, *236*, 313.
[25] A. Bentolila, I. Vlodavsky, C. Haloun, A. J. Domb, *Polym. Adv. Technol.* **2000**, *11*, 377.
[26] K. L. Christman, V. Vazquez-Dorbatt, E. Schopf, C. M. Kolodziej, R. C. Li, R. M. Broyer, Y. Chen, H. D. Maynard, *J. Am. Chem. Soc.* **2008**, *130*, 16585.
[27] H. Arwin, *Thin Solid Films* **1998**, *313*, 764.
[28] M. M. B. Nielsen, A. C. Simonsen, *Langmuir* **2013**, *29*, 1525.
[29] H. Krishna, R. Sachan, J. Strader, C. Favazza, M. Khenner, R. Kalyanaraman, *Nanotechnology* **2010**, *21*, 155601.
[30] J. Becker, G. Grun, R. Seemann, H. Mantz, K. Jacobs, K. R. Mecke, R. Blossey, *Nat. Mater.* **2003**, *2*, 59.
[31] S. Moungthai, T. H. Pham, A. Rajaendran, G. Stein, *Soft Matter* **2012**, *8*, 10026.
[32] P. Singh, C. Carraher, J. E. Schwarzbauer, *Annu. Rev. Cell Dev. Biol.* **2010**, *26*, 397.
[33] J. E. Schwarzbauer, D. W. DeSimone, *Cold Spring Harbor Perspect. Biol.* **2011**, *3*, a005041.
[34] J. E. Schwarzbauer, J. L. Sechler, *Curr. Opin. Cell Biol.* **1999**, *11*, 622.
[35] Y. Mao, J. E. Schwarzbauer, *Matrix Biol.* **2005**, *24*, 389.
[36] A. Barth, C. Zscherp, *Q. Rev. Biophys.* **2002**, *35*, 369.
[37] G. Baneyx, L. Baugh, V. Vogel, *Proc. Natl. Acad. Sci. USA* **2001**, *98*, 14464.
[38] M. L. Smith, D. Gourdon, W. C. Little, K. E. Kubow, R. A. Eguiluz, S. Luna-Morris, V. Vogel, *PLoS Biol.* **2007**, *5*, e268.
[39] E. Klotzsch, M. L. Smith, K. E. Kubow, S. Muntwyler, W. C. Little, F. Beyeler, D. Gourdon, B. J. Nelson, V. Vogel, *Proc. Natl. Acad. Sci. USA* **2009**, *106*, 18267.
[40] M. A. Hemphill, B. E. Dabiri, S. Gabriele, L. Kerscher, C. Franck, J. A. Goss, P. W. Alford, K. K. Parker, *PLoS One* **2011**, *6*, 1.
[41] B. Henderson, S. Nair, J. Pallas, M. A. Williams, *FEMS Microbiol. Rev.* **2011**, *35*, 147.
[42] E. Pauthe, J. Pelta, S. Patel, D. Lairez, F. Goubard, *Biochim. Biophys. Acta* **2002**, *1597*, 12.
[43] U. Ott, E. Odermatt, J. Engel, H. Furthmayr, R. Timpl, *Eur. J. Biochem.* **1982**, *123*, 63.
[44] L. Debelle, A. J. Alix, S. M. Wei, M. P. Jacob, J. P. Huvenne, M. Berjot, P. Legrand, *Eur. J. Biochem.* **1998**, *258*, 533.
[45] C. Petibois, G. Gouspillou, K. Wehbe, J.-P. Delage, G. Déléris, *Anal. Bioanal. Chem.* **2006**, *386*, 1961.
[46] C. Petibois, G. Deleris, *Trends Biotechnol.* **2006**, *24*, 455.
[47] H. Colognato, D. A. Winkelmann, P. D. Yurchenco, *J. Cell Biol.* **1999**, *145*, 619.
[48] K. E. Kadler, A. Hill, E. G. Canty-Laird, *Curr. Opin. Cell Biol.* **2008**, *20*, 495.
[49] K. Reiser, R. McCormick, R. Rucker, *FASEB J.* **1992**, *6*, 2439.
[50] K. E. Kadler, C. Baldock, J. Bella, R. P. Boot-Handford, *J. Cell Sci.* **2007**, *120*, 1955.
[51] L. Debelle, A. Tamburro, *Int. J. Biochem. Cell Biol.* **1999**, *31*, 261.
[52] A. Grosberg, P.-L. Kuo, C.-L. Guo, N. A. Geisse, M.-A. Bray, W. J. Adams, S. P. Sheehy, K. K. Parker, *PLoS Comput. Biol.* **2011**, *7*, e1001088.
[53] R. D. Lundberg, H. S. Makowski, G. H. Singhal, *US Patent 3 870 841*, **1975**.
[54] C. S. Chen, M. Mrksich, S. Huang, G. M. Whitesides, D. E. Ingber, *Science* **1997**, *276*, 1425.
[55] M. L. McCain, H. Lee, Y. Aratyn-Schaus, A. G. Kléber, K. K. Parker, *Proc. Natl. Acad. Sci. USA* **2012**, *109*, 9881.
[56] K. Shin, Y. Pu, M. H. Rafailovich, J. Sokolov, O. H. Seeck, S. K. Sinha, M. Tolan, R. Kolb, *Macromolecules* **2001**, *34*, 5620.
[57] P.-L. Kuo, H. Lee, M.-A. Bray, N. A. Geisse, Y.-T. Huang, W. J. Adams, S. P. Sheehy, K. K. Parker, *Am. J. Pathol.* **2012**, *181*, 2030.
[58] A. Dong, S. J. Prestrelski, S. D. Allison, J. F. Carpenter, *J. Pharm. Sci.* **1995**, *84*, 415.
[59] A. Dong, T. Lam, *Arch. Biochem. Biophys.* **2005**, *436*, 154.